ACS APPLIED MATERIALS & INTERFACES

Research Article

www.acsami.org

Effects of Immobilized BMP-2 and Nanofiber Morphology on In Vitro Osteogenic Differentiation of hMSCs and In Vivo Collagen Assembly of Regenerated Bone

Sajeesh Kumar Madhurakkat Perikamana,[†,‡] Jinkyu Lee,[†,‡] Taufiq Ahmad,[†,‡] Yonghoon Jeong,[§] Do-Gyoon Kim,[§] Kyobum Kim,*[,∥] and Heungsoo Shin*[,†,‡]

[†]Department of Bioengineering, Institute for Bioengineering and Biopharmaceutical Research, and [‡]BK21 Plus Future Biopharmaceutical Human Resources Training and Research Team, Hanyang University, Seoul 133-791, Republic of Korea

[§]Division of Orthodontics, College of Dentistry, The Ohio State University, Columbus, Ohio 43210, United States

[∥]Division of Bioengineering, College of Life Sciences and Bioengineering, Incheon National University, Incheon 406-772, Republic of Korea

Supporting Information

ABSTRACT: Engineering bone tissue is particularly challenging because of the distinctive structural features of bone within a complex biochemical environment. In the present study, we fabricated poly(L-lactic acid) (PLLA) electrospun nanofibers with random and aligned morphology immobilized with bone morphogenic protein-2 (BMP-2) and investigated how these signals modulate (1) in vitro osteogenic differentiation of human mesenchymal stem cells (hMSCs) and (2) in vivo bone growth rate, mechanical properties, and collagen assembly of newly formed bone. The orientation of adherent cells followed the underlying nanofiber morphology; however, nanofiber alignment did not show any difference in alkaline phosphate activity or in calcium mineralization of hMSCs after 14 days of in vitro culture in osteogenic differentiation media. In vivo bone regeneration was significantly higher in the nanofiber implanted groups (approximately 65−79%) as compared to the defect-only group (11.8 ± 0.2%), while no significant difference in bone regeneration was observed between random and aligned groups. However, nanoindentation studies of regenerated bone revealed Young's modulus and contact hardness with anisotropic feature for aligned group as compared to random group. More importantly, structural analysis of collagen at de novo bone showed the ability of nanofiber morphology to guide collagen deposition. SEM and TEM images revealed regular, highly ordered collagen assemblies on aligned nanofibers as compared to random fibers, which showed irregular, randomly organized collagen deposition. Taken together, we conclude that nanofibers in the presence of osteoinductive signals are a potent tool for bone regeneration, and nanofiber alignment can be used for engineering bone tissues with structurally assembled collagen fibers with defined direction.

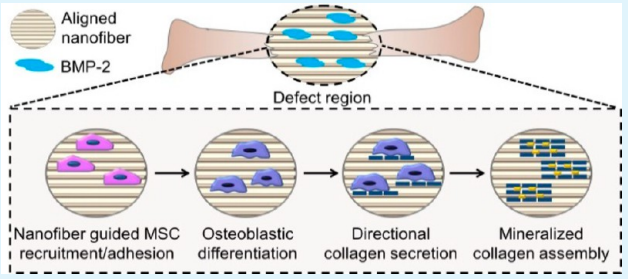

KEYWORDS: *bone tissue engineering, collagen assembly, contact guidance, electrospun nanofibers, bone morphogenic proteins*

INTRODUCTION

Bone tissue engineering has gained considerable interest in recent years due to various clinical issues and the limited availability of suitable bone grafts. Generally, natural bone healing is a multifactorial process that is orchestrated by many cell types and a variety of chemicals as well as physical signals.[1] At the earlier stages of bone healing, uncommitted mesenchymal stem cells migrate from the periosteum or bone marrow to the wound area and are then differentiated into osteoblasts by a group of growth factors including platelet derived growth factors and bone morphogenic proteins (BMPs).[2] The differentiated osteoblasts secrete type I collagen, which is mineralized in a later stage by chemical interactions with calcium and phosphate ions in the microenvironment, providing the main structural framework of bone tissue.[3] It has been reported that the mechanical property of bone depends on the volume of bone, the collagen mineral ratio, and the structural assembly of collagen at different hierarchical levels.[4] More importantly, collagen fibers are unidirectionally arranged (i.e., parallel to the long axis of the bone), and their structural features in the bone are vital for the increased tensile strength and load-bearing capacity of bone tissues.[5] Therefore, it is of importance to consider engineering methods to guide the structural assembly of collagen fibers in a bone microenvironment for regeneration of physiologically relevant bone tissue.

Most bone tissue engineering approaches have focused on developing biomaterials that are capable of recruiting and

Received: February 10, 2015
Accepted: March 31, 2015
Published: March 31, 2015

DOI: 10.1021/acsami.5b01340
ACS Appl. Mater. Interfaces 2015, 7, 8798−8808

inducing endogenous stem cell function.[6,7] A number of growth factors such as bone morphogenic proteins (BMP), vascular endothelial growth factor (VEGF), platelet derived growth factor (PDGF), or basic fibroblast growth factor (bFGF) have been used in bone engineering.[8−10] In particular, BMP-2 has attracted considerable attention because it is a potent inducer of both osteogenesis and angiogenesis during normal bone healing. Efforts have been made to develop the effective delivery of these growth factors to the defect site to mitigate problems associated with spatiotemporal distribution and optimal dosing of BMP-2 for the bone regeneration process.[11,12] The majority of delivery systems involve incorporation of BMP-2 within carrier materials that are engineered to release the BMP-2 to the defect in a soluble form to bind transmembrane receptors of bone forming cells. Alternatively, BMP-2 has been immobilized onto the surface of scaffolds via diverse chemical and physical methods to maintain long-term exposure to the microenvironment.[13,14] We reported immobilization of BMP-2 on PLLA nanofibers using polydopamine-inspired chemistry and revealed its potential in bone regeneration with controlled dosing.[15] Although these works provided insight into the use of inductive molecules for enhanced bone formation, unsolved questions still remain regarding how in vivo structural assembly of collagen is related to engineered bone.

Growing evidence indicates that the physical, architectural, and mechanical properties of scaffolds have tremendous influence on the in vitro activities of stem cells.[16] A variety of fabrication methods including micropatterning, 3D printing, and electrospinning have been used to introduce different structural features to biomaterials; the resulting diverse geometries including pits, pillars, or porous structure of scaffolds serve as critical signals to induce lineage-dependent behavior of stem cells.[17−19] Electrospinning has emerged as a potent tool in tissue engineering because it can easily produce fibrous structures with diameters ranging from a few hundred nanometers to submicrometers. Many researchers have explored nanofiber scaffolds in tissue engineering for skin, nerve, blood vessels, muscles, cartilage, and bone.[20−23] Furthermore, fiber physical properties such as alignment and diameter can be precisely controlled by changing the spinning parameters.[24] Aligned nanofibers have become an interesting platform for in vitro tissue engineering attempts because they can structurally mimic some of the native tissue organization. For instance, fibers with an aligned structure are effective for neuronal differentiation of embryonic stem cells, generation of longer myotubes in myoblasts, and even osteogenic differentiation behavior of different cell types.[25−29] However, the effect of these well-defined geometries from nanofibers on in vivo tissue formation, particularly the modulation of de novo collagen assembly during the bone healing process, has not yet been fully investigated.

The ultimate goal of this study was to develop ideal scaffolds for engineering bone tissues with well-controlled collagen assembly by understanding the structure−function relationship during the bone regeneration process. Our specific objectives were to analyze the synergistic or independent effects of nanofiber orientation and immobilized BMP-2 on (1) in vitro cell adhesion, morphology, and osteogenic behavior of human mesenchymal stem cells (hMSCs), (2) in vivo bone growth rate in a mouse calvarial critical size defect model, and (3) the mechanical properties and structural assemblies of collagen in regenerated bone tissues.

MATERIALS AND METHODS

PLLA was purchased from Boehringer Ingelheim GmbH (Resomer L214S, Essen, Germany, 5.7−8.5 dL/g viscosity). 1,1,1,3,3,3-Hexafluoro-2-propanol (HFIP) was from Wako (Osaka, Japan), and Tris-HCl was from Alfa Aesar (Heysham, UK). Phosphate buffered saline (PBS), fetal bovine serum (FBS), trypsin-ethylenediaminetetraacetic acid (TE), and penicillin-streptomycin (PS) were from Wisent (Montreal, QC, Canada). Dulbecco's modified eagle medium (DMEM) with low glucose was from Gibco BRL (Rockville, MD). Hoechst 33258 was from Molecular Probes (Eugene, OR), and rhodamine-phalloidin was from Invitrogen Corp. (Carlsbad, CA). Distilled water was produced by an Elix advantage system (Millipore, MA). Dopamine hydrochloride was from Sigma-Aldrich (St. Louis, MO). BMP-2 and BMP-2 Quantikine immunoassay kits were from R&D Systems (Minneapolis, MN). Unless otherwise specified, all other chemicals and solvents were obtained from Sigma-Aldrich.

Fabrication of PLLA Nanofibers and Characterization. Nanofibers with random and aligned morphology were fabricated using an electrospinning technique as previously reported.[30] Random fibers were collected using 2% PLLA solution in HFIP at a metal collector rotation speed of 200 rpm, and to collect aligned fibers the rotation speed of the collector was adjusted to 1400 rpm using 2.5% PLLA. The fabricated fibers were dried overnight at room temperature. The nanofibers were then coated with 2 mg/mL 3,4-dihydroxyphenethylamine (dopamine) dissolved in a 10 mM Tris buffer (pH 8.5) for 4 h with mild shaking. Nanofibers were rinsed and stirred in distilled water overnight to remove any unbound polydopamine. BMP-2 was immobilized on polydopamine-coated nanofibers by immersing the fibers in a solution of BMP-2 (500 ng/mL, 10 mM Tris-HCl buffer, pH 8.5) at 37 °C overnight, as previously reported.[15] Diameter of nanofibers and orientation angle were measured from SEM images (JEOL JSM 6330F, Tokyo, Japan) using Nikon imaging software (NIS-Elements AR 3.00, Nikon, Japan). The alignment of nanofibers was quantified by measuring the orientation angle of individual fibers from five images (n = 30). A reference angle was set by random selection, and the results were arranged into nine levels ranging from 0° to 90°. The frequency of nanofibers oriented in different angle ranges was calculated and presented as the percentage of total analyzed fibers. For quantifying the immobilized amount of BMP-2, nanofibers were treated with 500 μL of BMP-2 solution and incubated overnight at 37 °C and measured using enzyme-linked immunosorbent assay (ELISA). All ELISA experiments were performed according to the manufacturer's guidelines, and sample absorbance was measured using a spectrophotometer at 450 nm with 540 nm used for λ correction.

hMSCs Culture and Seeding on Nanofibers. The hMSCs used in this study were purchased from Cambrex Inc. (Charles City, IA), and they were expanded with growth media composed of low glucose DMEM, MEM, 10% FBS, and 1% PS under standard culture conditions (37 °C, 5% CO_2, and 95% humidity). For seeding onto nanofibers, circular samples (1.9 cm^2) were punched from random and aligned nanofibers and sterilized with 70% EtOH under UV light for 2 h. Sterilized samples were washed thoroughly with PBS and immobilized with BMP-2. The trypsinized hMSCs were then seeded onto the nanofibers at 2×10^4 cells/cm^2 for cell adhesion analysis and at 4×10^4 cells/cm^2 for all other in vitro experiments. After 1 day of incubation in growth media, cells were supplemented with osteogenic differentiation medium containing 10% FBS, 1% PS, 50 μg/mL ascorbic acid, 0.01 M glycerol-2-phosphate, and 10^{-7} M dexamethasone in low-glucose DMEM. The medium was changed every 2−3 days.

Cell Adhesion Analysis. Cell adhesion analysis on nanofibers was done using fluorescence staining and SEM imaging. After 1 day of incubation, the hMSCs on the nanofibers were washed twice with PBS and fixed using 4% paraformaldehyde. Fixed cells were stained for cell nuclei and F-actin using Hoechst 33258 (1:10 000) and rhodamine−phalloidin (1:200), respectively, in blocking buffer for 1 h at 37 °C. Images were acquired by confocal microscopy (LSM 5 Exciter, Carl Zeiss, Germany). Cell adhesion orientation was performed as for the nanofiber orientation. For each group, a total of 60 cells from different

DOI: 10.1021/acsami.5b01340
ACS Appl. Mater. Interfaces 2015, 7, 8798−8808

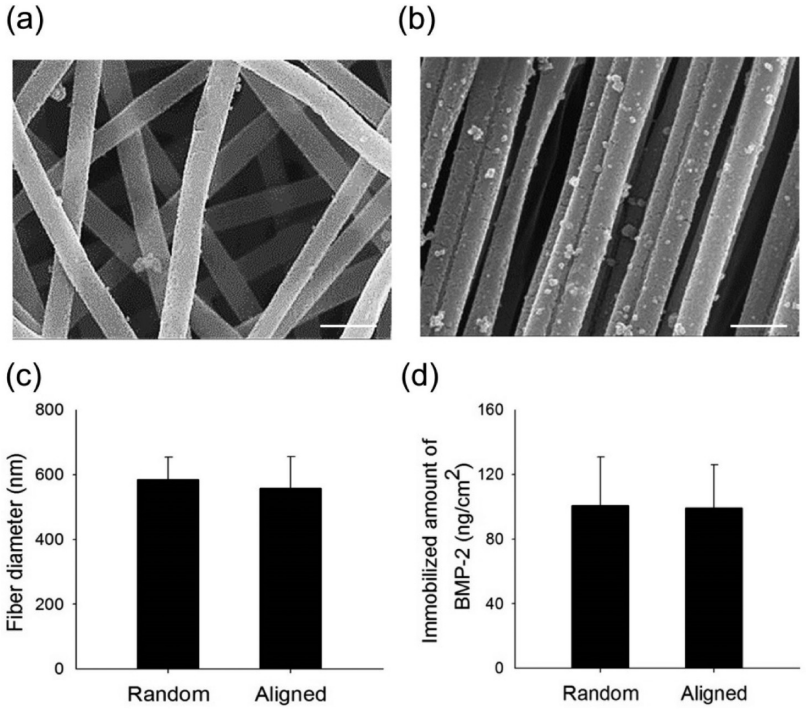

Figure 1. Characteristics of electrospun nanofibers. SEM images of (a) polydopamine coated random and (b) aligned nanofibers (scale bar: 1 μm). (c) Average diameter of polydopamine coated nanofibers and (d) the amount of immobilized BMP-2 on nanofibers.

images were analyzed and presented as a percentage of cells lying in a particular angle range to total analyzed cells. For SEM imaging, samples were treated with 1% glutaraldehyde for 30 min followed by 3 h in 4% formaldehyde. Samples were dehydrated through a series of graded alcohol solutions (30−100%). All samples were then treated with hexamethyldisilazane for 15 min and air-dried overnight. Prior to imaging, cells were gold coated using a sputter coater (BAL-TEC/SCD 005, BAL-TEC AG, Balzers, Liechtenstein) for 5 min and observed at an acceleration of 5 kV. For immunofluorescence staining with fibronectin, cells were fixed with 4% paraformaldehyde and permeabilized with cytoskeleton buffer and incubated with blocking buffer (5% FBS in PBS) for 1 h. Cells were then subsequently incubated with antifibronectin (1:200) for 1 h and then incubated with antimouse IgG biotin conjugate (1:200) and FITC-conjugated streptavidin (1:100) for 1 h. Cell nuclei were counter stained with Hoechst 33258.

In Vitro Osteogenic Differentiation Studies. hMSCs were cultured for 10 days under osteogenic differentiation medium, and ALP activity was measured using *p*-nitrophenyl phosphate (Sigma, St. Louis, MO) according to manufacturer's protocol. Lysed cell samples were centrifuged at 13 000*g* for 10 min, and 10 μL of collected supernatants were treated with 200 μL of *p*-nitrophenyl phosphate at 37 °C for 30 min. The reaction was stopped using 50 μL of 3 N NaOH, and the optical density was determined with spectrophotometer at 405 nm. A DNA assay was performed using the Quant-iT Pico Green ds DNA assay kit (Invitrogen, Carlsbad, CA) according to the manufacturer's procedure with the same set of samples. ALP activity was normalized to DNA content. To analyze the mineral deposition of hMSCs on both nanofibers, cells were cultured for 14 days in the osteogenic medium and quantified using the QuantiChrom Calcium Assay kit (Bioassay Systems, Hayward, CA) according to the manufacturer's instructions. Deposited calcium was estimated by spectrophotometrically measuring absorbance at 570−650 nm. Osteogenic differentiation studies on blank nanofibers (polydopamine-coated random and aligned nanofibers without BMP-2) were also calculated for analyzing the influence of nanofiber morphology without the presence of BMP-2.

Mouse Calvarial Defect Model. The effect of nanofiber morphology and immobilized BMP-2 on in vivo bone formation was assessed using 6-week-old ICR mice (Narabiothec, Seoul, Korea). All animal work was performed in accordance with protocols approved by the Institutional Animal Care and Use Committee (IACUC) at Hanyang University (HY-IACUC-12-079). Prior to operation, mice were anesthetized with xylazine (20 mg/kg) and Zoletil (60 mg/kg). Two, 4 mm sized defects were created on each side of the cranium using a suitable surgical trephine bur. The right side defect was covered with nanofibers, while the left side defect remained without any fiber implantation and served as the negative control. Surgery sites were sutured and treated with povidone iodine. Each group included four mice, and all mice were sacrificed after 2 months.

Micro-CT Analysis. New bone formation at the defect site was determined by micro-CT analysis. Mice were sacrificed using CO_2 gas, and skull bones were extracted. Bone samples were fixed with 10% neutral formalin for 3 days at 4 °C. Samples were exposed to micro-CT scanning (80 kV, 124 μA; Skyscan1172, Bruker-microct, Belgium), and three-dimensional images from micro-CT scanning were analyzed with Adobe Photoshop CS6 (Adobe Systems, CA) to measure regenerated bone areas.

Histological and Immunohistochemistry. For histological analysis, the skull bones underwent a decalcification process using Rapidcal (BBC Biochemical, Mount Vernon, WA) for 2 weeks with solution replacement every 2 days. Samples were dehydrated with graded EtOH (70−100%), toluene, and paraffin and embedded in paraffin wax and sectioned at 6 μm using a microtome (Shandon, Runcorn, Cheshire, GB). Sectioned samples were deparaffinized and hydrated and then stained for nuclei and cytosol with Harris hematoxylin and eosin solution. Goldner's trichrome staining method was performed to analyze collagen deposition in the defect area. Stained samples were dehydrated again, mounted with mounting medium (Richard-Allan Scientific, Kalamazoo, MI), and observed under an optical microscope (Nikon 2000, Japan). To analyze the presence of vascular structure on regenerated bone, tissue specimens were also immunostained with primary CD-31 specific antibodies. Samples were then visualized by treating with secondary antibodies, which are conjugated with FITC. Stained tissue specimens were then observed under a fluorescent microscope.

Mechanical Characterization. Nanoindentation method was used to analyze the elastic modulus and contact hardness of

DOI: 10.1021/acsami.5b01340
ACS Appl. Mater. Interfaces 2015, 7, 8798−8808

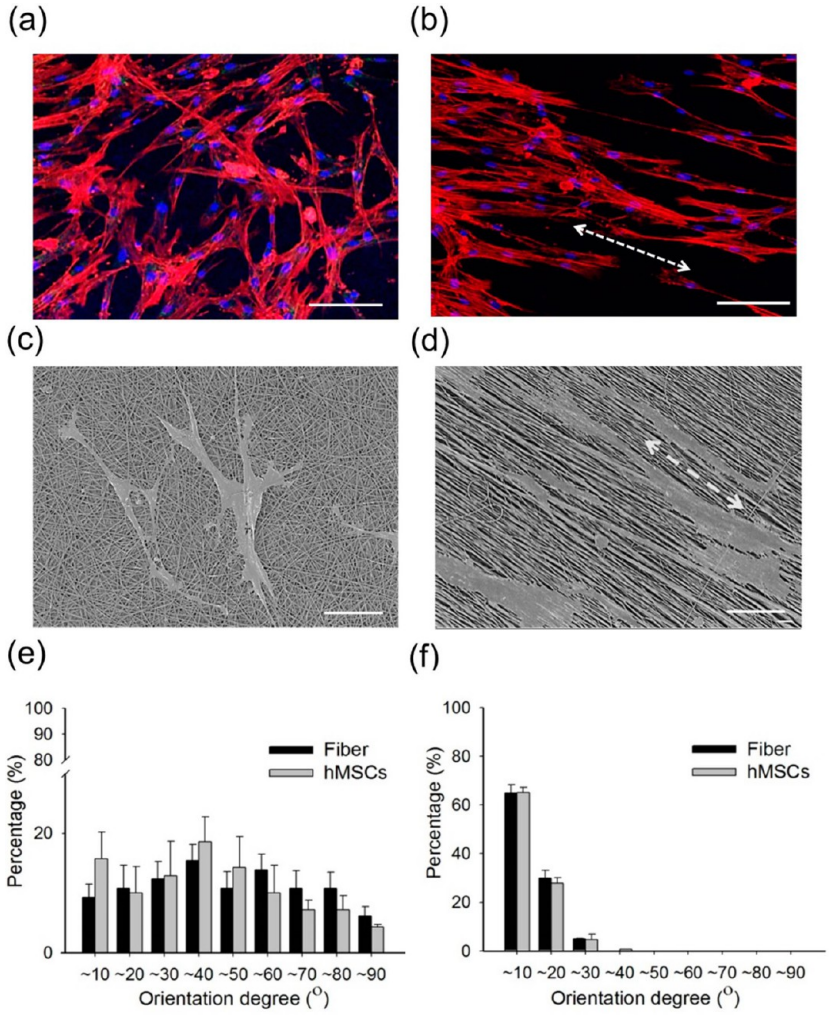

Figure 2. Adhesion of hMSCs on nanofibers. Fluorescence images stained for F-actin (red) and nuclei (blue) of hMSCs on (a) random and (b) aligned nanofibers after 24 h of culture (scale bar: 100 μm). SEM images of hMSCs on (c) random and (d) aligned nanofibers after 24 h of culture (scale bar: 20 μm). The orientation degree of adhered hMSCs and respective underlying (e) random and (f) aligned nanofibers. Dashed arrows indicate the mean direction of cell adhesion and aligned fibers.

regenerated bone tissue. Calvaria specimens were fixed and embedded with acrylic resin (Ortho-Jet, Lang, Wheeling, IL), and sectioned into 2 mm thickness slice with a low speed diamond saw (Isomet, Buehler, Lake Bluff, IL). The aligned specimens were cut horizontal and vertical to the fiber direction. Sections were polished using silicon carbide abrasive paper and aluminum oxide paste and glued onto a stainless steel holder and mounted on a nanoindenter (Nano-XP, MTS, Oakridge, TN). All indentations were conducted up to 500 nm depth with loading and unloading displacement rates of 10 nm/s following the previous study.[31] The indentation force−displacement curves then were used to obtain the contact hardness by dividing the peak indentation force by the projected area at the end of loading, and the elastic modulus using the unloading slope. The distance between indent locations was at least 30 μm to avoid any interruptions from the adjacent indents. A total of 363 nanoindentation sites were analyzed including 185 at the regenerated bone tissues and 178 at the host bone tissues.

SEM and TEM Imaging. Scanning electron microscopy (SEM) and transmission electron microscopy (TEM) imaging were performed to analyze the deposited collagen fiber morphology at the defect site. Implanted nanofibers were cut in the perpendicular direction to the bone regeneration direction to confirm fiber direction. The procedure for SEM imaging was the same as for in vitro SEM imaging, and morphology was observed by field emission scanning electron microscopy (FE-SEM) (AURIGA, Carl Zeiss, Germany). For TEM imaging, samples underwent transition by treating them with 100% propylene oxide, and they were embedded with Spurr's resin through polymerization at 70 °C. Embedded samples were sectioned by ultramicrotome (MT-X, RMC, Tucson, AZ), stained with 2% uranyl acetate and Reynolds' lead citrate for 7 min, and observed by TEM (LIBRA 120, Carl Zeiss, Germany). Nanofiber circularity was calculated from TEM images of implanted fibers (50 individual fibers for each group) using Nikon imaging software (NIS-Elements AR 3.00, Nikon, Japan) and presented as the percentage of fibers that lay in different circularity levels to total analyzed fibers. For quantification of the collagen aspect ratio, zoomed TEM images were used, and an aspect ratio of 35 individual collagen fibers was analyzed by calculating the long axis/short axis using ImageJ software.

Statistical Analysis. Quantitative values are shown as the average ± standard error of the average, and the data were analyzed using *t* test or ANOVA with Tukey HSD procedure. Values of $p < 0.05$ were considered significant.

RESULTS AND DISCUSSION

Nanofiber Characterization. Many recent studies have shared information on the influence of physical properties of biomaterials on tuning cell behavior in ex vivo conditions. However, this information poorly translates to in vivo environments. In the present study, we analyzed the

DOI: 10.1021/acsami.5b01340
ACS Appl. Mater. Interfaces 2015, 7, 8798−8808

importance of structural cues in bone tissue engineering using electrospun nanofibers. To provide structural guidance for in vitro and in vivo experiments, PLLA nanofibrous scaffolds with random and aligned morphologies were fabricated and studied in the in vitro osteogenic differentiation of hMSCs and in vivo bone regeneration in a mouse calvarial defect model.

SEM images clearly showed a difference in morphology for the two types of nanofibers (Figure 1a and b). An irregular woven arrangement of nanofibers was found in random fiber groups, whereas a highly aligned ordered distribution of individual fibers was observed for the aligned nanofibers. The average fiber diameter in both groups was similar at 500−600 nm (Figure 1c) and is similar to that of individual collagen fibers in the bone extracellular microenvironment.[32] A faster rotation speed of the collector (1500 rpm) resulted in stretching of the fibers in the direction of the collector, which gave highly unidirectional nanofibers. In contrast, spinning the fibers at a lower rotation speed (200 rpm) resulted in randomly aligned nanofibers, which was consistent with previous studies.[25,33] The amount of coated dopamine (data not given) and immobilized BMP-2 on nanofibers showed no difference between the random and aligned fiber groups (Figure 1d). Quantified BMP-2 was 100.5 ± 0.3 and 99.2 ± 0.2 ng/cm^2 on random and aligned fibers, respectively. Polydopamine coating was presented as a powerful tool in cell/tissue engineering in recent years due to its versatility and ease of use.[34−36] In our previous work, we found an excellent immobilization efficiency (nearly 90%) of BMP-2 on nanofibers using polydopamine chemistry, and the long-term presence of osteoinductive BMP-2 facilitated in vivo bone regeneration.[15] The amines and thiols present in the biomolecules can be reacted with catecholamine-containing polydopamine through Michael addition or Schiff base reactions.[37,38] To confirm the specific interaction of amines and thiols in the BMP-2 to the polydopamine layer, we analyzed immobilization efficiency of BMP-2 on polydopamine-coated nanofibers at different pH values of tris-HCl such as pH 4, 7, and 8.5 (Supporting Information Figure S1). It was found that BMP-2 immobilized on polydopamine-coated nanofibers at pH 8.5 showed the highest immobilization efficiency among tested groups. In general, Michael addition and Schiff base reactions involved in thiols and amines show the highest reaction efficiency at slight alkaline pH.[39,40] Hence, pH 8.5 would have facilitated the strong covalent interaction between BMP-2 and polydopamine. In order words, as the pH reduced, the interaction between BMP-2 and polydopamine also diminished. Nanofibers, in which BMP-2 was immobilized at pH 4, showed the least interaction. At this pH, polydopamine possesses a net positive charge because of the protonation of the amine group, which may further nullify any chance of electrostatic interactions between positively charged BMP-2.[41]

Cell Adhesion and Morphology. Cell adhesion behavior in the random and aligned groups was investigated by fluorescent staining and SEM imaging (Figure 2a−d). hMSCs showed sufficient cell adhesion and widely spread cell morphology on both types of fibers with notable difference. On random fibers, hMSCs were more polygonal in shape and distributed randomly throughout the nanofibers. On aligned fibers, the cells had spindle shape morphology and stretched along the long axis of the underlying nanofibers. The orientation of adherent cells as compared to that of individual fibers on different nanofiber alignments was analyzed (Figure 2e and f). In the aligned nanofiber group, an orientation degree of ∼65% of the cells was within <10°, which suggests unidirectional adhesion of hMSCs along the underlying nanofibers. On the random nanofiber group, an irregular distribution of orientation degree (1−90°) of individual fibers and cells was observed.

The change in cell adhesion and elongated cellular morphology on nanofibrous scaffolds can be explained by the classical theory of contact guidance.[42] Different cell types, including endothelial cells, neuronal cells, cardiomyocytes, and hMSCs, received contact guidance cues from the underlying substrate such as nano-/micropatterned substrates and nanofibers.[25,43,44] Aligned nanofibers have recently been explored to employ spatial instruction for different stem cells types. Embryonic stem cells were cultured on aligned poly(ε-caprolactone) and showed a very elongated morphology that resembles the structure of neuronal cell types.[45] When human unrestricted somatic stem cells were cultured on aligned poly-ε-caprolactone/poly-L-lactic acid/hydroxyapatite nanofibers, the same morphological changes were observed as we reported.[46] Well-organized fibronectin assembly was observed after 10 days of culture in an osteogenic medium, which followed the same trend of initial cell adhesion. Fibronectin is one of the main components in the bone extracellular matrix, second to collagen type 1. It is conceivable that cells may prefer to continue their initial cell adhesion behavior and that ECM secretion can also follow the same pattern, which is consistent with other studies.[28]

Osteogenic Differentiation of hMSCs. We observed that hMSCs on both orientations of fibers showed similar levels of osteogenic differentiation irrespective of fiber morphology as well as cell morphology. Immuno-stained images showed organized assemblies of fibronectin on both types of nanofibers. Moreover, preferred cell adhesion was consistent with day one culture as the fibronectin assembly was also found to follow the fiber orientation (Figure 3a and b). We then analyzed the osteogenic differentiation potential of hMSCs on random and aligned fibers (Figure 3c and d). We found that there was no difference in osteogenic differentiation between the groups. ALP activity on random fibers and aligned fibers was 2.4 ± 0.1 and 2.4 ± 0.2 nmol/DNA/30 min, respectively. Analysis of calcium content also showed the same trend as calcium; content in the random group was 45.8 ± 1 μg and in the aligned group was 45.0 ± 1 μg. However, in the non-BMP-2 immobilized nanofiber groups, aligned nanofibers showed higher osteogenic differentiation properties than did random nanofiber groups (Supporting Information Figure S2).

In general, different physical factors such as surface topography, stiffness, and shear stress are influential in osteogenic differentiation of different cells, although osteogenic differentiation on random and aligned nanofibers is slightly controversial.[47] For example, Liu et al. demonstrated that human bone marrow mesenchymal stem cells (hBMSCs) cultured on PLLA fibers showed increased ALP activity and higher expression of osteogenic genes on random fibers as compared to an aligned substrate.[27] Contrary to these results, bone marrow stromal cells grown on aligned PLGA-based scaffolds showed higher expression of osteogenic gene markers such as RUNX2 and OSX.[28] Similarly, increased ALP activity and calcium content as well as higher expression of Runx-2, COL-1, and OCN were observed on PCL/COL-1 aligned nanofibers.[48] In our study, only polydopamine-coated nanofibers (without immobilized BMP-2) showed reduced osteogenic differentiation capacity as compared to the BMP-2

DOI: 10.1021/acsami.5b01340
ACS Appl. Mater. Interfaces 2015, 7, 8798−8808

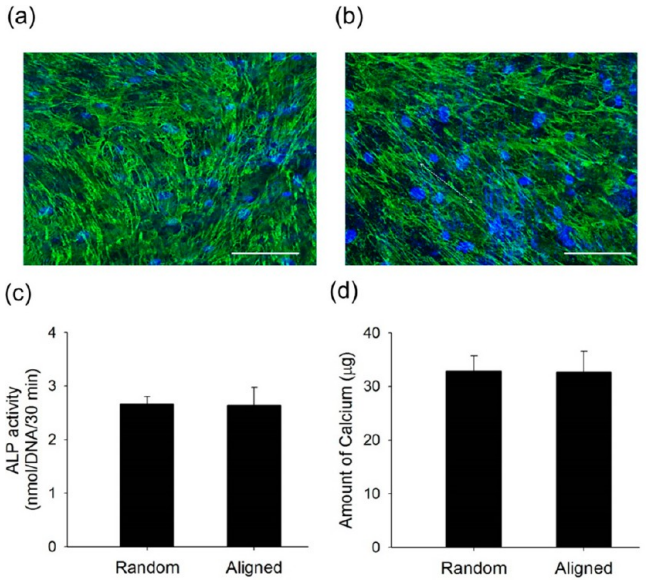

Figure 3. Osteogenic differentiation studies on nanofibers. Immunofluorescence images of hMSCs on (a) random and (b) aligned nanofibers showing the nucleus (blue) and fibronectin (green) assembly after 10 days of culture in osteogenic culture medium (scale bar: 100 μm). (c) ALP activity of cultured hMSCs on nanofibers after 10 days. (d) Quantification of mineralized calcium by hMSCs cultured on nanofibers after 14 days.

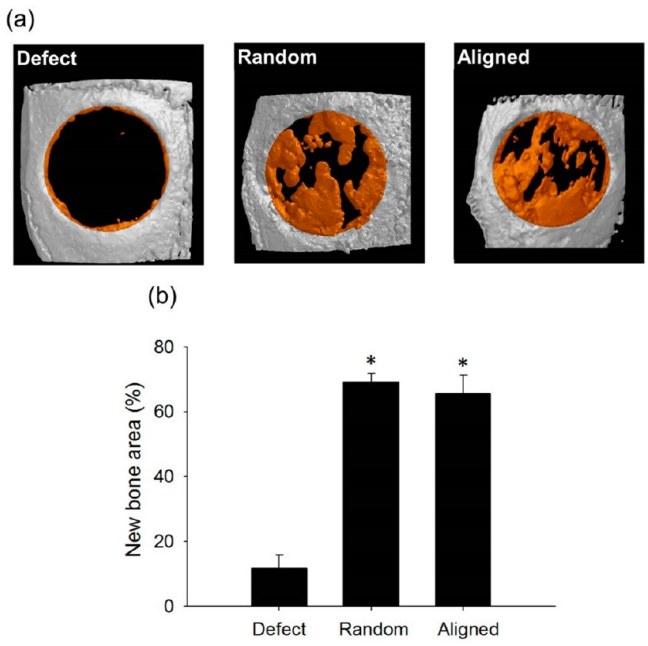

Figure 4. Radiographic analysis of skull bone implanted with random and aligned nanofibers 2 months after surgery. (a) The micro-CT images of the various nanofibers from the implanted skull bone samples and (b) the quantitative values of regenerated new bone area from each group. The "*" indicates a significant difference as compared to the defect-only group ($p < 0.05$).

immobilized groups. Notably, aligned nanofibers in the non-BMP-2 immobilized groups showed higher ALP and calcium activity than that of random nanofiber groups, but random and aligned nanofibers with immobilized BMP-2 showed no difference. It should be noted that most of the above-mentioned studies were conducted on substrates without any modification using inductive chemical factors. In contrast, we immobilized a strong osteoinductive factor, BMP-2, on the surface of the nanofibers with the aid of polydopamine, and we speculate that the alignment of nanofibers may be influential when there is no strong chemical signal; however, the influence of physical factors may become less significant in the presence of a strong chemical signal (BMP-2).

In Vivo Bone Formation and Histology. New bone formation was analyzed on implanted nanofibers in a calvarial defect model after 2 months using micro CT (Figure 4a). Bone regeneration in both the random nanofiber and the aligned fiber groups was increased (69.2 ± 0.1% and 65.7 ± 0.4%, respectively) as compared to the defect-only group (11.8 ± 0.2%) (Figure 4b). H&E staining showed the rich encapsulation of host cells and thick tissue formation along the implanted nanofiber region with the presence of regenerated blood vessels (black arrows) as compared to the defect-only group (Supporting Information Figure S3a–c). Goldner's trichrome staining demonstrated a dense distribution of regenerated collagen fibers throughout the defect region for both nanofiber groups (Figure 5a–c). The nanofibers were completely covered by newly formed thick collagen fibers, which were integrated into the host tissues. Large blood vessels and lacunae (black arrows) were also observed throughout the regenerated tissues. The immunohistochemistry of implanted samples showed CD-31 marker expression on random and aligned nanofibers, which confirmed the presence of vascular structure on newly generated bone tissues (Supporting Information Figure S3a–c).

Overall, the bone regeneration in the BMP-2 immobilized nanofiber groups was significantly enhanced relative to the defect-only group, which is consistent with our previous study.[15] Histological and immunofluorescent images of sectioned samples showed the presence of blood vessels throughout the nanofiber region, which further showed the maturation of newly formed bone at the defect site. It has been indicated that BMP-2 can also indirectly influence the neovascular structure formation.[49] Hence, along with the bone regeneration, BMP-2 would have also triggered the formation of blood vessels in de novo bone tissues. However, consistent with our in vitro results, we did not observe any difference in overall bone growth between the random and aligned groups. In general, migration of osteoblasts or progenitor cells from the neighboring region to the defect site is affected by (1) gradients in concentration of growth factors and (2) geometrical patterns of bone ECM. In a recent study from our group, aligned PLLA fibers enhanced both the in vitro migration speed of hMSCs and in vivo bone regeneration as compared to random fibers.[30] Nevertheless, in this study, both the random and the aligned groups showed a similar level of in vivo bone regeneration when BMP-2 was conjugated to the substrate fibrous scaffolds. As speculated from our in vitro results, the presence of BMP-2 may be more decisive than geometrical factors (i.e., orientation of substrate fibers) in recruiting progenitors and osteoblasts in the in vivo bone microenvironment. To the best of our knowledge, it is the first study investigating the effect of both fiber alignment and the presence of growth factors in the in vivo guided bone regeneration applications.

Mechanical Properties of New Bone. Modulus and hardness of the newly regenerated bone on defect-only group and nanofiber implanted group were measured using nanoindentation and compared to host native bone (Figure 6a). For the regenerated bone tissue in the nanofiber groups, their

DOI: 10.1021/acsami.5b01340
ACS Appl. Mater. Interfaces 2015, 7, 8798–8808

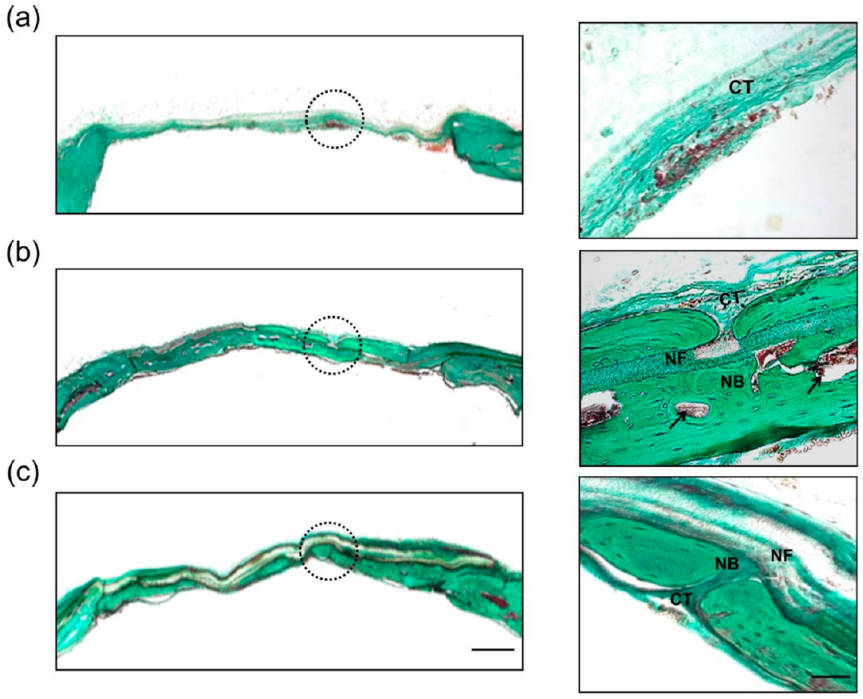

Figure 5. Histological analysis of sectioned mouse calvaria. The defect model samples 2 months after nanofiber implantation. Goldener's trichome staining images of (a) the defect-only group, (b) the random nanofiber implanted group, and (c) the aligned nanofiber implanted group. Magnified images of dotted circles from each figure are presented at the right side (scale bar: 50 μm). Black arrows, newly generated blood vessels in regenerated bone (CT = connective tissue, NF = nanaofiber, NB = new bone).

elastic moduli in the horizontal direction were comparable to those for the corresponding host bone tissues ($p > 0.49$) (Figure 6b). On the other hand, the elastic modulus in the vertical direction for the regenerated bone tissue in the aligned nanofiber group was significantly lower than that for its corresponding host bone tissue (13.68 ± 2.55 GPa vs 15.67 ± 3.27 GPa) ($p = 0.002$). The contact hardness in the horizontal direction for the regenerated bone tissue in the aligned nanofiber group was significantly higher than that for its corresponding host bone tissue (0.52 ± 0.1 GPa vs 0.45 ± 0.09 GPa) ($p = 0.019$), while other nanofiber groups had comparable values with those of the corresponding host bone tissues ($p > 0.264$) (Figure 6c). However, mechanical properties of bone tissue regenerated at the defect site were significantly less as compared to the corresponding host bone tissue and the regenerated bone tissues in all other groups ($p < 0.001$) having an elastic modulus of 3.80 ± 0.95 GPa and contact hardness of 0.12 ± 0.05 GPa.

Most of the guided bone regeneration studies have concentrated on analyzing the bone regeneration capacity of the implanted biomaterials. However, the long-term success of implants may lie on the functionality of the newly regenerated bone, which may be defined by how closely it mimics the native bone, both functionally and structurally. Bone is a highly anisotropic and viscoelastic material that can withstand a high level of mechanical loading. Hence, it is important to analyze the mechanical properties of newly regenerated bone to understand its functional properties. Elastic modulus and contact hardness of the bone at the nanoscale level may depend on the structural assembly and degree of mineralization of collagen.[50] Our nanoindentation studies showed that the mechanical property of regenerated bone at the nanofiber implanted groups was significantly higher than the defect-only group, and those values were close to that of host bone, implying that regenerated bone facilitated by our implanted nanofiber exhibited bone characteristics and was functionally close to the host bone. Histological analysis demonstrated that thick collagen deposition and deposited collagen along with mineralization may have resulted in physiologically matching mechanical properties. Interestingly, regenerated tissue at the aligned nanofiber groups showed anisotropic mechanical behaviors. Young's modulus was slightly lower in the vertical direction, whereas contact hardness in the vertical direction was slightly higher as compared to the corresponding host bone. Many of the previous studies have shown directional-dependent mechanical behavior of different bone tissues.[51,52] Together, we conclude that our BMP-2 immobilized nanofibers at the defect site facilitated matured bone characteristics with mechanical properties similar to those of the host bone, and aligned nanofibers showed an anisotropic mechanical behavior similar to that of the natural bone tissues.

Structural Assembly of Collagen. We performed SEM and TEM analysis of the implanted nanofibers to analyze the structural assembly of collagen in the newly regenerated bone. The SEM images clearly depict the impact of fiber morphology on controlling the collagen fiber deposition characteristics (Figure 7a–d). Nonuniformly arranged collagen fibers were deposited on random nanofibers, and these randomly deposited collagen bundles structurally resemble woven bone characteristics.[3] In contrast, a regular, ordered, unidirectional distribution of collagen fibers was observed in regenerated bone tissues in the aligned nanofiber group. It is important to note that the individual collagen fibers were more closely packed on aligned nanofibers than on the random fibers, and they formed relatively thicker collagen bundles. These aligned collagen bundles were well organized and ran parallel to the long axis of

DOI: 10.1021/acsami.5b01340
ACS Appl. Mater. Interfaces 2015, 7, 8798–8808

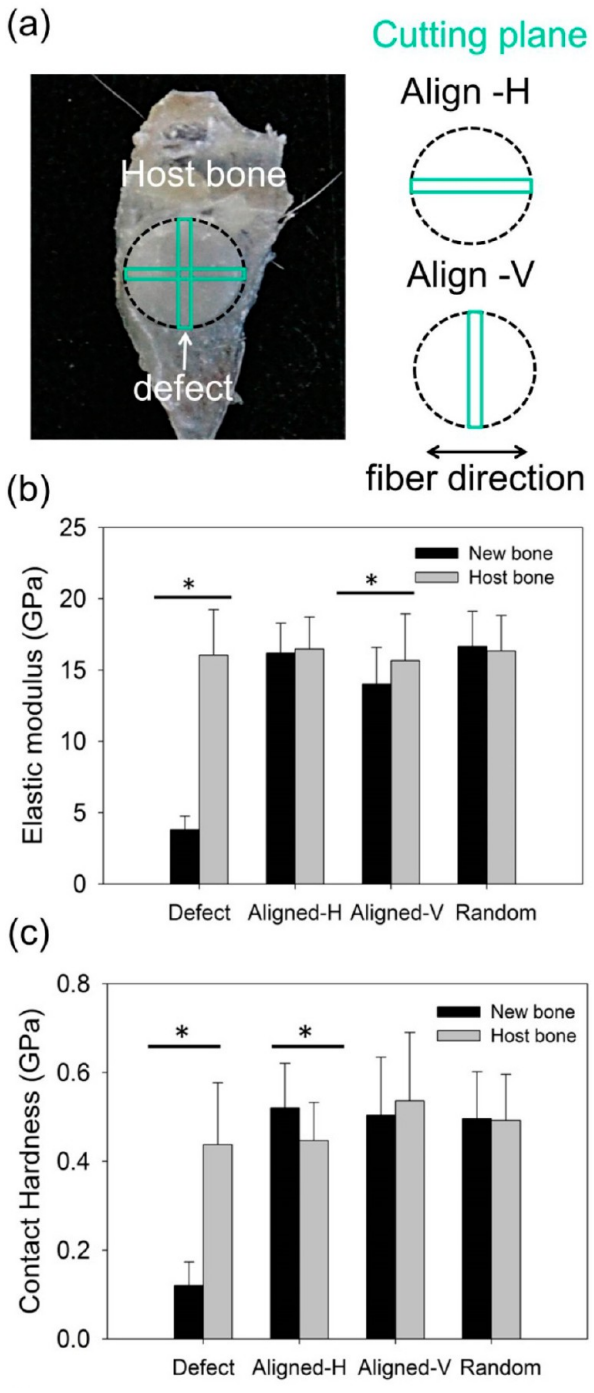

Figure 6. Mechanical characterization of newly regenerated bone using nanoindentation. (a) Cutting direction for the implanted aligned nanofiber group, (b) elastic modulus of different groups as compared to that of host bone, and (c) contact hardness of the different groups as compared to that of host bone. The "*" indicates a significant difference as compared to the corresponding host bone group ($p < 0.05$).

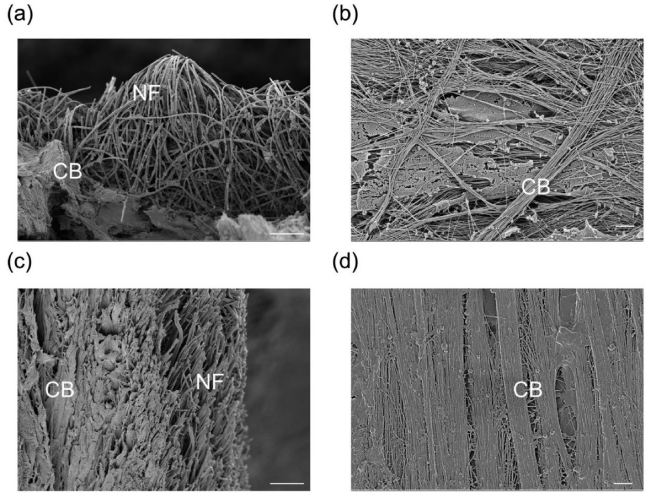

Figure 7. SEM images of calvaria tissues at 2 months postimplantation of nanofibers. Lower and higher magnification images of (a) implanted, (b) random, and (c and d) aligned groups (NF, nanofiber; CB, collagen bundle). Scale bars represent 10 μm for (a) and (c), and 2 μm for (b) and (d).

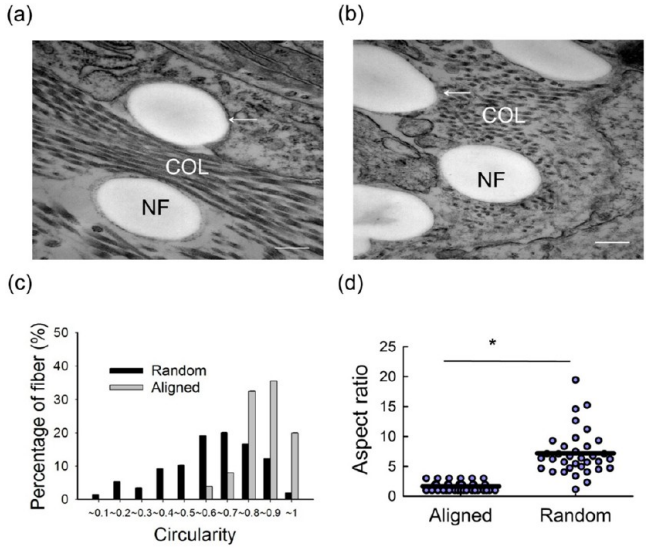

Figure 8. TEM images of calvarial tissues 2 months postimplantation of nanofibers. Images of (a) random nanofiber groups and (b) aligned nanofiber groups. (c) Circularity of implanted nanofibers and (d) aspect ratio of newly regenerated collagen fibers were analyzed (NF, nanofiber; COL, collagen). White arrows indicate the presence of coated collagen on the nanofibers. Scale bar represents 200 nm. The "*" indicates a significant difference as compared to the defect-only group ($p = 0.0000002892$).

the nanofibers without any impedance. This observation clearly indicates that collagen deposition was strongly affected by underlying fiber morphology.

The orientation of the deposited collagen matrix was further confirmed by TEM imaging (Figure 8a–d). The images showed a strong interaction of nanofibers with the surrounding regenerated tissue. In the aligned nanofiber group, the collagen fibers were observed as circular dots, indicating uniformity in the orientation of deposited collagen fibers. To make sure that implanted nanofibers maintained their respective morphologies, the circularity of individual nanofibers was also analyzed; samples were cut perpendicular to the bone regeneration direction. The semiqualitative data of nanofiber circularity showed that the majority of nanofiber circularity in the aligned nanofibers was close to one, indicating unidirectional alignment of fibers. In contrast, the circularity of the random nanofibers was distributed throughout the range of 0.1–1, which confirmed the irregular orientation of the nanofibers. The aspect ratio of individual collagen fibers indicates a heteroge-

DOI: 10.1021/acsami.5b01340
ACS Appl. Mater. Interfaces 2015, 7, 8798–8808

neous distribution of values, which indicates the randomness of the collagen fiber orientation in the random fiber groups. Collagen fibers in the aligned nanofiber groups showed reduced aspect ratio values with a narrow distribution.

Bone is a highly dynamic tissue that is continuously remodeled during its normal growth or following injury. Woven bone is initially produced during bone remodeling and is characterized by a mechanically weak, disorganized arrangement of collagen fibers. However, during the bone remodeling process, woven bone is eventually replaced by regular, parallel aligned collagen fibers that form a sheet-like structure called lamellar bone. There is recent evidence that the structure of the implanted biomaterials can influence the collagen deposition pattern.[53] In this study, we observed that collagen remodeling was strictly controlled by the nanofiber architecture. A lamellar-like collagen assembly was found on aligned nanofibers, whereas a disorganized, woven-like pattern was observed on the random fibers during the same time period. Under natural conditions, bone remodeling is a function of the response of the bone to external mechanical loading (Wolf's law). However, under load-free conditions such as biomaterial-based approaches, nanofiber alignment can influence collagen remodeling during bone healing. Here, we propose a possible mechanism of in vivo collagen matrix assembly guided by implanted aligned fibers (Figure 9). The presence of BMP-2 on

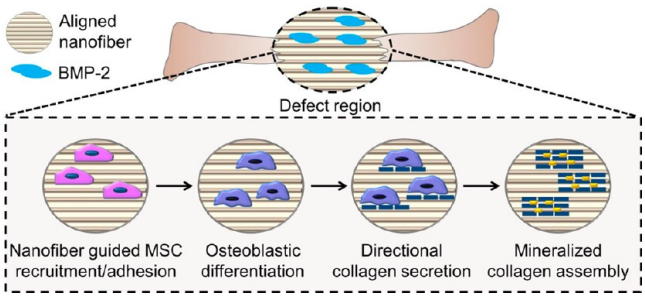

Figure 9. Schematic mechanism of in vivo collagen assembly as instructed by the implanted aligned nanofibers.

the implanted nanofibers actively turns endogenous progenitor cells into osteoblasts where, through contact guidance, their adhesion is instructed by the nanofiber morphology. The osteoblasts then secrete collagen along the direction of cell adhesion (fiber direction), which subsequently forms the collagen fibril bundles in the direction of deposited collagen molecules. Individual collagen fibrils may undergo directional mineralization and then be grouped together to make collagen fibers resulting in the fiber direction-dependent anisotropic mechanical properties of the regenerated bone tissues as observed in this study. These mineralized structures are then assembled together to form an organized structure of bone. On the basis of this proposed model, we conclude that, along with the right chemical cues, smart structural designing may also be needed for biomaterial-based bone tissue engineering.

CONCLUSIONS

In this study, we used BMP-2 immobilized electrospun PLLA nanofibers with random and aligned morphologies to test the combinatorial effects of biochemical and structural cues on in vitro osteogenic differentiation of hMSCs and in vivo bone regeneration in a mouse calvarial defect model. Cell adhesion and ECM assembly in vitro were directed by the underlying nanofiber morphology, while fiber alignment did not have a significant influence on in vitro osteogenic differentiation. In addition, overall in vivo bone regeneration was similar on both fiber groups, and it was significantly greater as compared to the defect-only control groups, implying that surface immobilized BMP-2 actively induced new bone formation. The mechanical properties of newly regenerated bone on both fibers were close to those of host bone at the micro scale level; more importantly, anisotropic characteristics in Young's modulus and contact harness were demonstrated only in the groups that received aligned nanofibers. Observation of tissue specimen using SEM and TEM revealed that nanofiber alignment was able to direct structural assembly of newly regenerated collagen fibers at the defect site. Aligned nanofibers showed ordered, unidirectional alignment of collagen assembly that resembled collagen assembly of a lamellar bone, which also resulted in anisotropic mechanical behavior. Together, our results suggest that biochemical factors (e.g., BMP-2) may have more influence on bone regeneration; however, structural properties of biomaterials (nanofiber alignment) can control collagen fiber assembly and thereby may be used to engineer structurally relevant bone.

ASSOCIATED CONTENT

Supporting Information

Figures showing immobilization of BMP-2 on polydopamine substrate at different pH values of tris-HCl, osteogenic differentiation of hMSCs on blank and BMP-2 immobilized random and aligned fibers, and expression of angiogenic markers on implanted nanofibers. This material is available free of charge via the Internet at http://pubs.acs.org.

AUTHOR INFORMATION

Corresponding Authors

*Tel.: +82-32-835-8297. Fax: +82-32-835-0804. E-mail: kyobum.kim@inu.ac.kr.

*Tel.: +82-2-2220-2346. Fax: +82-2-2298-2346. E-mail: hshin@hanyang.ac.kr.

Notes

The authors declare no competing financial interest.

ACKNOWLEDGMENTS

This work was supported by a National Research Foundation of Korea (NRF) grant funded by the Korea government (MEST) (NRF-2013R1A2A2A03067809) and the Incheon National University Research Grant in 2014.

REFERENCES

(1) Jahagirdar, R.; Scammell, B. E. Principles of Fracture Healing and Disorders of Bone Union. *Surgery (Oxford)* **2009**, *27*, 63−69.

(2) Mehta, M.; Schmidt-Bleek, K.; Duda, G. N.; Mooney, D. J. Biomaterial Delivery of Morphogens to Mimic the Natural Healing Cascade in Bone. *Adv. Drug Delivery Rev.* **2012**, *64*, 1257−1276.

(3) Kini, U.; Nandeesh, B. Physiology of Bone Formation, Remodeling, and Metabolism. *Radionuclide and Hybrid Bone Imaging*; Springer: New York, 2012; pp 29−57.

(4) Viguet-Carrin, S.; Garnero, P.; Delmas, P. The Role of Collagen in Bone Strength. *Osteoporosis Int.* **2006**, *17*, 319−336.

(5) Ramasamy, J.; Akkus, O. Local Variations in the Micromechanical Properties of Mouse Femur: The Involvement of Collagen Fiber Orientation and Mineralization. *J. Biomech.* **2007**, *40*, 910−918.

(6) Stevens, M. M. Biomaterials for Bone Tissue Engineering. *Mater. Today* **2008**, *11*, 18−25.

DOI: 10.1021/acsami.5b01340
ACS Appl. Mater. Interfaces 2015, 7, 8798−8808

(7) Murphy, C. M.; O'Brien, F. J.; Little, D. G.; Schindeler, A. Cell-Scaffold Interactions in the Bone Tissue Engineering Triad. *Eur. Cells Mater.* **2013**, *26*, 120−132.
(8) Aryal, R.; Chen, X. p.; Fang, C.; Hu, Y. c. Bone Morphogenetic Protein-2 and Vascular Endothelial Growth Factor in Bone Tissue Regeneration: New Insight and Perspectives. *Orthop. Surg.* **2014**, *6*, 171−178.
(9) Lee, J.-h.; Lee, Y. J.; Cho, H.-j.; Kim, D. W.; Shin, H. The Incorporation of Bfgf Mediated by Heparin into Pcl/Gelatin Composite Fiber Meshes for Guided Bone Regeneration. *Drug Delivery Transl. Res.* **2015**, *5*, 146−159.
(10) Delgado, J.; Sánchez, E.; Baro, M.; Reyes, R.; Évora, C.; Delgado, A. A Platelet Derived Growth Factor Delivery System for Bone Regeneration. *J. Mater. Sci.: Mater. Med.* **2012**, *23*, 1903−1912.
(11) Zara, J. N.; Siu, R. K.; Zhang, X.; Shen, J.; Ngo, R.; Lee, M.; Li, W.; Chiang, M.; Chung, J.; Kwak, J. High Doses of Bone Morphogenetic Protein 2 Induce Structurally Abnormal Bone and Inflammation in Vivo. *Tissue Eng., Part A* **2011**, *17*, 1389−1399.
(12) Boerckel, J. D.; Kolambkar, Y. M.; Dupont, K. M.; Uhrig, B. A.; Phelps, E. A.; Stevens, H. Y.; García, A. J.; Guldberg, R. E. Effects of Protein Dose and Delivery System on Bmp-Mediated Bone Regeneration. *Biomaterials* **2011**, *32*, 5241−5251.
(13) Bae, S. E.; Choi, J.; Joung, Y. K.; Park, K.; Han, D. K. Controlled Release of Bone Morphogenetic Protein (Bmp)-2 from Nanocomplex Incorporated on Hydroxyapatite-Formed Titanium Surface. *J. Controlled Release* **2012**, *160*, 676−684.
(14) Li, L.; Zhou, G.; Wang, Y.; Yang, G.; Ding, S.; Zhou, S. Controlled Dual Delivery of Bmp-2 and Dexamethasone by Nanoparticle-Embedded Electrospun Nanofibers for the Efficient Repair of Critical-Sized Rat Calvarial Defect. *Biomaterials* **2015**, *37*, 218−229.
(15) Cho, H.-j.; Madhurakkat Perikamana, S. K.; Lee, J.-h.; Lee, J.; Lee, K.-M.; Shin, C. S.; Shin, H. Effective Immobilization of Bmp-2 Mediated by Polydopamine Coating on Biodegradable Nanofibers for Enhanced in Vivo Bone Formation. *ACS Appl. Mater. Interfaces* **2014**, *6*, 11225−11235.
(16) Ozdemir, T.; M Higgins, A.; L Brown, J. Osteoinductive Biomaterial Geometries for Bone Regenerative Engineering. *Curr. Pharm. Des.* **2013**, *19*, 3446−3455.
(17) Kim, D.-H.; Provenzano, P. P.; Smith, C. L.; Levchenko, A. Matrix Nanotopography as a Regulator of Cell Function. *J. Cell Biol.* **2012**, *197*, 351−360.
(18) Kim, K.; Dean, D.; Wallace, J.; Breithaupt, R.; Mikos, A. G.; Fisher, J. P. The Influence of Stereolithographic Scaffold Architecture and Composition on Osteogenic Signal Expression with Rat Bone Marrow Stromal Cells. *Biomaterials* **2011**, *32*, 3750−3763.
(19) Wang, X.; Song, W.; Kawazoe, N.; Chen, G. The Osteogenic Differentiation of Mesenchymal Stem Cells by Controlled Cell−Cell Interaction on Micropatterned Surfaces. *J. Biomed. Mater. Res., Part A* **2013**, *101*, 3388−3395.
(20) Dhandayuthapani, B.; Krishnan, U. M.; Sethuraman, S. Fabrication and Characterization of Chitosan-Gelatin Blend Nanofibers for Skin Tissue Engineering. *J. Biomed. Mater. Res., Part B* **2010**, *94*, 264−272.
(21) Biazar, E.; Keshel, S. H.; Pouya, M.; Rad, H.; Nava, M. O.; Azarbakhsh, M.; Hooshmand, S. Nanofibrous Nerve Conduits for Repair of 30-Mm-Long Sciatic Nerve Defects. *Neural Regener. Res.* **2013**, *8*, 2266.
(22) Sankaran, K. K.; Subramanian, A.; Krishnan, U. M.; Sethuraman, S. Nanoarchitecture of Scaffolds and Endothelial Cells in Engineering Small Diameter Vascular Grafts. *Biotechnol. J.* **2015**, *10*, 96−108.
(23) Eap, S.; Morand, D.; Clauss, F.; Huck, O.; Stoltz, J.-F.; Lutz, J.-C.; Gottenberg, J.-E.; Benkirane-Jessel, N.; Keller, L.; Fioretti, F. Nanostructured Thick 3d Nanofibrous Scaffold Can Induce Bone. *Biomed. Mater. Eng.* **2015**, *25*, 79−85.
(24) Luo, C.; Stoyanov, S. D.; Stride, E.; Pelan, E.; Edirisinghe, M. Electrospinning Versus Fibre Production Methods: From Specifics to Technological Convergence. *Chem. Soc. Rev.* **2012**, *41*, 4708−4735.
(25) Corey, J. M.; Lin, D. Y.; Mycek, K. B.; Chen, Q.; Samuel, S.; Feldman, E. L.; Martin, D. C. Aligned Electrospun Nanofibers Specify the Direction of Dorsal Root Ganglia Neurite Growth. *J. Biomed. Mater. Res., Part A* **2007**, *83*, 636−645.
(26) Choi, J. S.; Lee, S. J.; Christ, G. J.; Atala, A.; Yoo, J. J. The Influence of Electrospun Aligned Poly (ε-Caprolactone)/Collagen Nanofiber Meshes on the Formation of Self-Aligned Skeletal Muscle Myotubes. *Biomaterials* **2008**, *29*, 2899−2906.
(27) Liu, W.; Wei, Y.; Zhang, X.; Xu, M.; Yang, X.; Deng, X. Lower Extent but Similar Rhythm of Osteogenic Behavior in Hbmscs Cultured on Nanofibrous Scaffolds Versus Induced with Osteogenic Supplement. *ACS Nano* **2013**, *7*, 6928−6938.
(28) Lyu, S.; Huang, C.; Yang, H.; Zhang, X. Electrospun Fibers as a Scaffolding Platform for Bone Tissue Repair. *J. Orthop. Res.* **2013**, *31*, 1382−1389.
(29) Kolambkar, Y. M.; Bajin, M.; Wojtowicz, A.; Hutmacher, D. W.; García, A. J.; Guldberg, R. E. Nanofiber Orientation and Surface Functionalization Modulate Human Mesenchymal Stem Cell Behavior in Vitro. *Tissue Eng., Part A* **2013**, *20*, 398−409.
(30) Lee, J.-h.; Lee, Y. J.; Cho, H.-j.; Shin, H. Guidance of in Vitro Migration of Human Mesenchymal Stem Cells and in Vivo Guided Bone Regeneration Using Aligned Electrospun Fibers. *Tissue Eng., Part A* **2013**, *20*, 2031−2042.
(31) Kim, D.-G.; Huja, S. S.; Lee, H. R.; Tee, B. C.; Hueni, S. Relationships of Viscosity with Contact Hardness and Modulus of Bone Matrix Measured by Nanoindentation. *J. Biomech. Eng.* **2010**, *132*, 024502.
(32) Parenteau-Bareil, R.; Gauvin, R.; Berthod, F. Collagen-Based Biomaterials for Tissue Engineering Applications. *Materials* **2010**, *3*, 1863−1887.
(33) Kai, D.; Prabhakaran, M. P.; Jin, G.; Ramakrishna, S. Guided Orientation of Cardiomyocytes on Electrospun Aligned Nanofibers for Cardiac Tissue Engineering. *J. Biomed. Mater. Res., Part B* **2011**, *98*, 379−386.
(34) Shin, Y. M.; Lee, Y. B.; Shin, H. Time-Dependent Mussel-Inspired Functionalization of Poly (L-Lactide-Co-ε-Caprolactone) Substrates for Tunable Cell Behaviors. *Colloids Surf., B* **2011**, *87*, 79−87.
(35) Shin, Y. M.; Jun, I.; Lim, Y. M.; Rhim, T.; Shin, H. Bio-Inspired Immobilization of Cell-Adhesive Ligands on Electrospun Nanofibrous Patches for Cell Delivery. *Macromol. Mater. Eng.* **2013**, *298*, 555−564.
(36) Shin, Y. M.; Lee, Y. B.; Kim, S. J.; Kang, J. K.; Park, J.-C.; Jang, W.; Shin, H. Mussel-Inspired Immobilization of Vascular Endothelial Growth Factor (Vegf) for Enhanced Endothelialization of Vascular Grafts. *Biomacromolecules* **2012**, *13*, 2020−2028.
(37) LaVoie, M. J.; Ostaszewski, B. L.; Weihofen, A.; Schlossmacher, M. G.; Selkoe, D. J. Dopamine Covalently Modifies and Functionally Inactivates Parkin. *Nat. Med.* **2005**, *11*, 1214−1221.
(38) Lee, H.; Dellatore, S. M.; Miller, W. M.; Messersmith, P. B. Mussel-Inspired Surface Chemistry for Multifunctional Coatings. *Science* **2007**, *318*, 426−430.
(39) Mather, B. D.; Viswanathan, K.; Miller, K. M.; Long, T. E. Michael Addition Reactions in Macromolecular Design for Emerging Technologies. *Prog. Polym. Sci.* **2006**, *31*, 487−531.
(40) Zhou, L.; Chen, M.; Guan, Y.; Zhang, Y. Multiple Responsive Hydrogel Films Based on Dynamic Schiff Base Linkages. *Polym. Chem.* **2014**, *5*, 7081−7089.
(41) Yu, B.; Liu, J.; Liu, S.; Zhou, F. Pdop Layer Exhibiting Zwitterionicity: A Simple Electrochemical Interface for Governing Ion Permeability. *Chem. Commun.* **2010**, *46*, 5900−5902.
(42) Driscoll, M. K.; Sun, X.; Guven, C.; Fourkas, J. T.; Losert, W. Cellular Contact Guidance through Dynamic Sensing of Nanotopography. *ACS Nano* **2014**, *8*, 3546−3555.
(43) Wise, J. K.; Yarin, A. L.; Megaridis, C. M.; Cho, M. Chondrogenic Differentiation of Human Mesenchymal Stem Cells on Oriented Nanofibrous Scaffolds: Engineering the Superficial Zone of Articular Cartilage. *Tissue Eng., Part A* **2008**, *15*, 913−921.
(44) Gupta, D.; Venugopal, J.; Prabhakaran, M. P.; Dev, V.; Low, S.; Choon, A. T.; Ramakrishna, S. Aligned and Random Nanofibrous Substrate for the in Vitro Culture of Schwann Cells for Neural Tissue Engineering. *Acta Biomater.* **2009**, *5*, 2560−2569.

DOI: 10.1021/acsami.5b01340
ACS Appl. Mater. Interfaces 2015, 7, 8798−8808

(45) Xie, J.; Willerth, S. M.; Li, X.; Macewan, M. R.; Rader, A.; Sakiyama-Elbert, S. E.; Xia, Y. The Differentiation of Embryonic Stem Cells Seeded on Electrospun Nanofibers into Neural Lineages. *Biomaterials* **2009**, *30*, 354−362.
(46) Bakhshandeh, B.; Soleimani, M.; Ghaemi, N.; Shabani, I. Effective Combination of Aligned Nanocomposite Nanofibers and Human Unrestricted Somatic Stem Cells for Bone Tissue Engineering. *Acta Pharmacol. Sin.* **2011**, *32*, 626−636.
(47) Chen, J. C.; Jacobs, C. R. Mechanically Induced Osteogenic Lineage Commitment of Stem Cells. *Stem Cell Res. Ther.* **2013**, *4*, 107.
(48) Chen, X.; Fu, X.; Shi, J.-g.; Wang, H. Regulation of the Osteogenesis of Pre-Osteoblasts by Spatial Arrangement of Electrospun Nanofibers in Two-and Three-Dimensional Environments. *Nanomedicine* **2013**, *9*, 1283−1292.
(49) Dyer, L. A.; Pi, X.; Patterson, C. The Role of Bmps in Endothelial Cell Function and Dysfunction. *Trends Endocrinol. Metab.* **2014**, *25*, 472−480.
(50) Gourion-Arsiquaud, S.; Burket, J. C.; Havill, L. M.; DiCarlo, E.; Doty, S. B.; Mendelsohn, R.; van der Meulen, M. C.; Boskey, A. L. Spatial Variation in Osteonal Bone Properties Relative to Tissue and Animal Age. *J. Bone Miner. Res.* **2009**, *24*, 1271−1281.
(51) Novitskaya, E.; Chen, P.-Y.; Lee, S.; Castro-Ceseña, A.; Hirata, G.; Lubarda, V. A.; McKittrick, J. Anisotropy in the Compressive Mechanical Properties of Bovine Cortical Bone and the Mineral and Protein Constituents. *Acta Biomater.* **2011**, *7*, 3170−3177.
(52) Seto, J.; Gupta, H. S.; Zaslansky, P.; Wagner, H. D.; Fratzl, P. Tough Lessons from Bone: Extreme Mechanical Anisotropy at the Mesoscale. *Adv. Funct. Mater.* **2008**, *18*, 1905−1911.
(53) Scaglione, S.; Giannoni, P.; Bianchini, P.; Sandri, M.; Marotta, R.; Firpo, G.; Valbusa, U.; Tampieri, A.; Diaspro, A.; Bianco, P. Order Versus Disorder: In Vivo Bone Formation within Osteoconductive Scaffolds. *Sci. Rep.* **2012**, *2*, 274.

DOI: 10.1021/acsami.5b01340
ACS Appl. Mater. Interfaces 2015, 7, 8798−8808